molecules

MDPI

Article

Evaluation of a Nondestructive NMR and MRI Method for Monitoring the Drying Process of *Gastrodia elata* Blume

Yannan Chen [1,2], Hongjing Dong [1], Jingkun Li [1], Lanping Guo [3,*] and Xiao Wang [1,2,*]

1 Key Laboratory of TCM Quality Control Technology, Shandong Analysis and Test Center, Qilu University of Technology (Shandong Academy of Sciences), Jinan 250014, China; 18954530681@163.com (Y.C.); donghongjing_2006@163.com (H.D.); ljk2091@163.com (J.L.)
2 College of Food Science and Engineering, Shandong Agricultural University, Tai'an 270018, China
3 Resource Center of Chinese Materia Medica, State Key Laboratory Breeding Base of Dao-di Herbs, China Academy of Chinese Medical Sciences, Beijing 100700, China
* Correspondence: glp01@126.com (L.G.); wangx@sdas.org (X.W.); Tel.: +86-10-64089808 (L.G.); +86-531-82605319 (X.W.)

Received: 11 December 2018; Accepted: 8 January 2019; Published: 10 January 2019

Abstract: *Gastrodia elata* Blume (*G. elata*) is a prominent traditional herb and its dry tuber is officially listed in the Chinese Pharmacopoeia. To ensure the quality of dried *G. elata*, the establishment of a nondestructive and convenient method to monitor the drying process is necessary. In this study, a nondestructive low-field nuclear magnetic resonance (LF-NMR) and magnetic resonance imaging (MRI) method was introduced to monitor the drying process of *G. elata*. Three water states (bound, immobilized, and free) in *G. elata* samples were investigated through multiexponential fitting and inversion of the NMR data. The variation and distribution of the three water states during drying were monitored by LF-NMR, and the spatial distribution of water and internal structural changes were analyzed by MRI. Linear analysis of the moisture content, L^* (lightness), b^* (yellowness), and NMR parameters showed good correlations among them. Furthermore, partial least squares regression (PLSR) model analysis, which takes into account all NMR parameters, also showed good correlations among these parameters. All results showed that LF-NMR was feasible and convenient for monitoring moisture content. Therefore, LF-NMR and MRI could be used to monitor the moisture content nondestructively in the drying process of Chinese traditional herbs.

Keywords: *Gastrodia elata* Blume; drying; LF-NMR; MRI; water variation; chemometric analysis

1. Introduction

Drying is an indispensable step in Chinese herbal medicine processing and is important for ensuring the quality [1]. Drying causes water evaporation to achieve the required moisture content and inhibits the biochemical reactions and proliferation of microorganisms [2]. Therefore, the drying degree (or moisture content) directly affects herb quality. Traditional methods for measuring the moisture content of Chinese herbal medicines include the weight method, differential scanning calorimetry, and near-infrared spectroscopy [3,4]. However, most of these methods are tedious, time-consuming, and interrupt the drying process. To reduce the drying time and obtain Chinese herbal medicines of good quality, it is necessary to develop a rapid and nondestructive method for analyzing water variations during the drying process.

Low-field nuclear magnetic resonance (LF-NMR) is a powerful tool for analyzing water variation in food owing to its nondestructive characteristics, rapid analysis speed, and low cost [5,6]. By measuring the proton relaxation times, the state, distribution, activity, and mobility of water can

be determined using LF-NMR [7–10]. Magnetic resonance imaging (MRI), the other type of NMR technology, has been used to detect the internal distribution of water and structural changes during processing [11]. In recent years, combining NMR with MRI has been widely used to analyze food processing. Geng et al. [12] and Zhang et al. [13] have used both NMR and MRI to study dried sea cucumber rehydration and monitor the natto fermentation process, respectively. LF-NMR and MRI are also sensitive methods for monitoring water variation during drying processes. Cheng et al. [14] and Xu et al. [15] studied the water variation in shrimp and broccoli during drying, successfully applying these measurements to ensure food quality. However, there is no suitable method for analyzing the drying process of Chinese herbal medicines. Therefore, the development of a rapid and nondestructive analytical method for the Chinese herbal medicine industry would be extremely significant.

Gastrodia elata Blume (*G. elata*) is a prominent traditional herb used in many Asian countries [16]. The dry tuber of *G. elata* is officially listed in the Chinese Pharmacopoeia and has a beneficial effect on headaches, paralysis, rheumatism, and other nervous disorders [17–19]. To process *G. elata*, it must first be steamed and then dried to obtain high-quality pieces [20]. Therefore, monitoring the drying process of *G. elata* is important to obtain high-quality products. In this study, a nondestructive NMR and MRI method was introduced to monitor the drying process of *G. elata* by investigating water variation and internal structural changes. The relationships between moisture content, NMR parameters, and color parameters were investigated through linear analysis. Partial least squares regression (PLSR) analysis, taking into account all NMR parameters, was also applied. This NMR and MRI method could also potentially be applied to other Chinese herbal medicines.

2. Results and discussion

2.1. Effects of Steaming on Water States and Distribution

Steaming *G. elata* is beneficial for drying [21]. Figure 1 shows the transverse relaxation time (T_2) curves of fresh *G. elata* and *G. elata* after steaming. T_2 reflects the chemical environment of protons and degree of water freedom in the sample [22]. The *G. elata* relaxation time curves showed three peaks, namely, T_{21} (0.1–10 ms), T_{22} (10–200 ms), and T_{23} (200–1000 ms) from left to right. These peaks represent the three molecular environments in which water molecules existed, where T_{21} corresponds to water binding closely to the macromolecular particles, T_{22} corresponds to water binding in the cytoplasm, and T_{23} corresponds to free water in the vacuole and intercellular space with strong mobility [23]. The corresponding signal amplitudes were A_{21}, A_{22}, and A_{23}, respectively, representing the relative moisture contents of the three states.

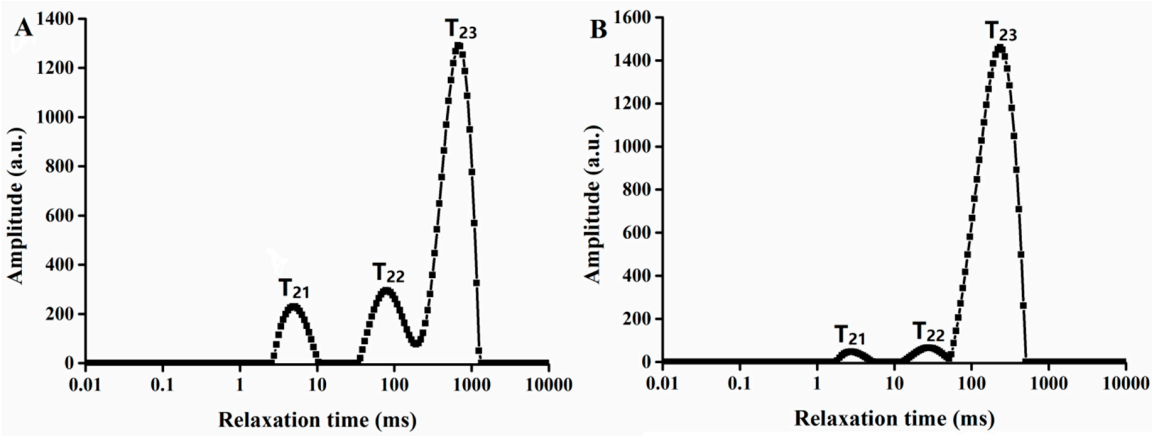

Figure 1. LF-NMR T_2 relaxation time distribution curves of *G. elata* (**A**) before steaming and (**B**) after steaming.

Table 1 shows changes in the relaxation time and peak area of *G. elata* before and after steaming. After steaming, A_{21}, A_{22}, and A_{23} had all changed significantly, and the free water content had increased

from 70.88% to 95.45%. Meanwhile, the bound water content had decreased from 11.11% to 1.62% and the content of immobilized water had decreased from 18.01% to 2.93%. These results indicated that the structure of *G. elata* was damaged by steaming, with water diffusing to the outside owing to differences between the internal and external pressures, while the free water content clearly increased.

Table 1. Changes in relaxation time and peak area of *G. elata* before and after steaming.

	A_{21} (%)	A_{22} (%)	A_{23} (%)	T_{21} (ms)	T_{22} (ms)	T_{23} (ms)
Before steaming	11.11 ± 0.3^a	18.01 ± 0.5^a	70.88 ± 0.4^a	5.18 ± 0.5^a	96.81 ± 0.4^a	584.94 ± 0.4^a
After steaming	1.62 ± 0.2^b	2.93 ± 0.6^b	95.45 ± 0.5^b	5.39 ± 0.3^a	89.59 ± 0.5^b	274.18 ± 0.6^b

[a] Values are means ± standard deviation (n = 3). [b] Different letters in the same column indicate a significant difference ($p < 0.05$).

Figure 2 shows cross-sectional MRI images of *G. elata* before and after steaming, where different colors represent different water contents [24]. From the color strip, red represents the highest moisture content and blue represents the lowest moisture content [25]. The water distribution inside *G. elata* was uneven before steaming, with the moisture content increasing gradually from inside to outside. The tissue structure was damaged after steaming, which accelerated the space movement of internal moisture, and the moisture distribution became uniform. These results demonstrated that steaming accelerated the drying rate.

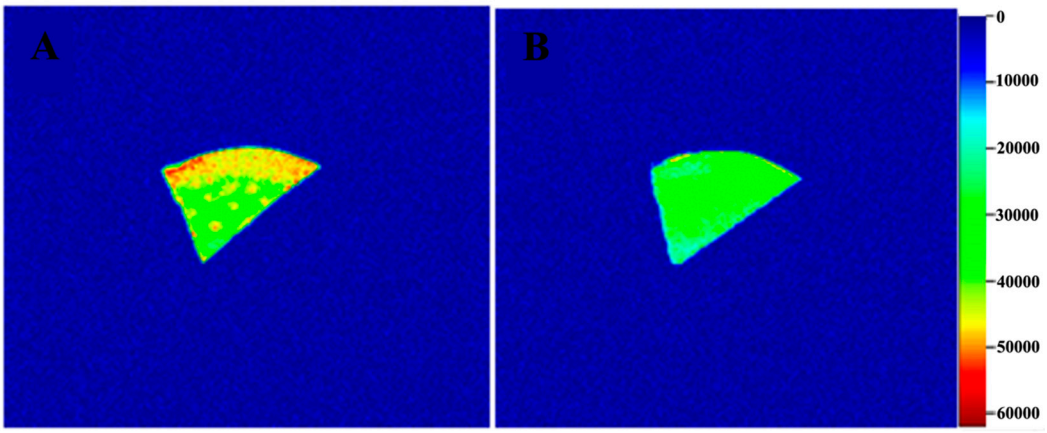

Figure 2. Cross-sectional MRI images of *G. elata* (**A**) before steaming and (**B**) after steaming.

2.2. Transverse Relaxation Time Analysis of G. elata after Steaming at Different Drying Temperatures

Figure 3 shows the transverse relaxation time curves of *G. elata* after steaming at different drying temperatures. The drying process changes the water content and states, and can also alter the water binding forces with macromolecules [26]. The peak area gradually decreased and the position of each peak gradually moved to the left. Meanwhile, the degree of water binding with non-water components became increasingly close, and the relaxation time gradually decreased.

Changes in the relaxation time and peak area of *G. elata* (after steaming) dried at 40, 60, and 80 °C are shown in Tables 2–4, which explain the changes in water states on the microscale. During the drying process, T_{21} values showed little change in the ranges 0.53–5.03 ms at 40 °C, 0.69–4.69 ms at 60 °C, and 0.93–4.20 ms at 80 °C. This indicated that bound water was tightly combined with the macromolecular substances and not easily removed during drying. The T_{22} and T_{23} values showed a significant decreasing trend with drying, which might be due to destruction of the cell membrane during drying. Macromolecules, such as polysaccharides, in *G. elata* flow into the intercellular space and increase the solution concentration, which increases opportunities for the combination of macromolecules with water that has poor mobility [27].

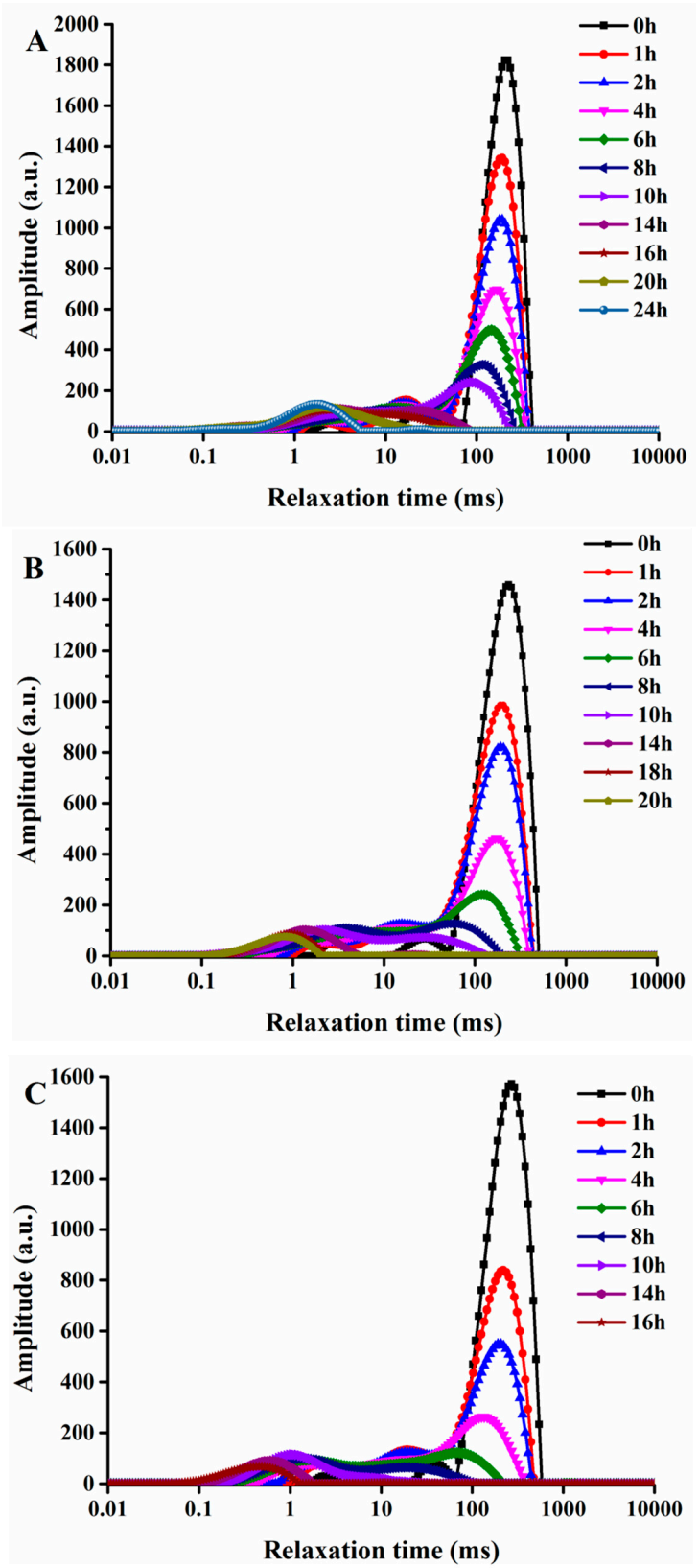

Figure 3. Transverse relaxation time curves of *G. elata* after steaming at different drying temperatures of (**A**) 40 °C, (**B**) 60 °C, and (**C**) 80 °C.

Table 2. Changes in relaxation time and peak area of *G. elata* dried at 40 °C after steaming.

Drying Time (min)	T_{21} (ms) [1,2]	T_{22} (ms) [1,2]	T_{23} (ms) [1,2]	A_{21}/g [1,2]	A_{22}/g [1,2]	A_{23}/g [1,2]	A_{Total}/g [1,2]
2	5.03 ± 0.15^{a}	83.66 ± 4.66^{a}	248.94 ± 3.65^{a}	48.01 ± 1.91^{f}	86.75 ± 3.22^{e}	2210.86 ± 4.25^{a}	2345.62 ± 6.23^{a}
4	4.47 ± 0.19^{b}	75.14 ± 5.31^{b}	234.98 ± 4.60^{b}	55.03 ± 3.56^{f}	99.04 ± 2.45^{d}	2015.86 ± 14.60^{b}	2169.93 ± 4.26^{b}
6	3.99 ± 0.21^{c}	62.12 ± 4.57^{c}	215.61 ± 3.73^{c}	70.58 ± 4.04^{e}	110.32 ± 4.08^{c}	1878.33 ± 9.48^{c}	2059.23 ± 3.58^{c}
8	3.27 ± 0.20^{d}	53.42 ± 2.61^{d}	200.47 ± 4.26^{d}	86.37 ± 4.41^{d}	125.50 ± 3.97^{b}	1650.33 ± 13.51^{d}	1862.20 ± 3.22^{d}
10	2.82 ± 0.14^{e}	44.71 ± 3.07^{e}	186.46 ± 2.99^{e}	100.57 ± 4.08^{c}	142.13 ± 2.78^{a}	1433.37 ± 9.11^{e}	1676.08 ± 8.21^{e}
12	2.26 ± 0.26^{f}	36.79 ± 2.86^{f}	172.90 ± 6.29^{f}	118.61 ± 6.25^{b}	124.58 ± 4.20^{b}	1116.68 ± 10.21^{f}	1359.87 ± 6.58^{f}
14	1.63 ± 0.17^{g}	30.83 ± 1.33^{fg}	155.35 ± 5.23^{g}	135.29 ± 4.12^{a}	95.40 ± 4.06^{d}	882.68 ± 6.94^{g}	1113.37 ± 7.66^{g}
16	1.21 ± 0.22^{h}	25.23 ± 1.64^{gh}	136.09 ± 3.15^{h}	108.95 ± 4.15^{c}	104.71 ± 4.69^{f}	544.84 ± 9.52^{h}	758.50 ± 6.23^{h}
18	0.96 ± 0.08^{hi}	21.03 ± 1.55^{hi}	121.28 ± 1.56^{i}	73.95 ± 4.56^{e}	56.61 ± 3.17^{g}	212.35 ± 7.67^{i}	342.91 ± 5.02^{i}
20	0.76 ± 0.06^{ij}	18.05 ± 1.36^{i}	-	51.66 ± 2.63^{f}	32.85 ± 1.86^{h}	-	84.51 ± 2.18^{j}
22	0.53 ± 0.08^{j}	-	-	33.81 ± 3.33^{g}	-	-	33.81 ± 1.47^{k}

[1] Values are means ± standard deviation (n = 3). [2] Different letters in the same column indicate a significant difference ($p < 0.05$).

Table 3. Changes in relaxation time and peak area of *G. elata* dried at 60 °C after steaming.

Drying Time (min)	T_{21} (ms) [1,2]	T_{22} (ms) [1,2]	T_{23} (ms) [1,2]	A_{21}/g [1,2]	A_{22}/g [1,2]	A_{23}/g [1,2]	A_{Total}/g [1,2]
2	4.69 ± 0.35^{a}	79.83 ± 5.47^{a}	243.61 ± 4.48^{a}	50.35 ± 4.09^{f}	89.75 ± 4.03^{d}	2129.84 ± 4.88^{a}	2269.94 ± 12.43^{a}
4	4.13 ± 0.60^{ab}	70.13 ± 6.28^{b}	226.65 ± 3.32^{b}	58.03 ± 3.91^{f}	102.37 ± 2.34^{c}	1734.84 ± 8.75^{b}	1895.25 ± 7.83^{b}
6	3.69 ± 0.48^{b}	59.77 ± 3.09^{c}	208.94 ± 2.63^{c}	75.253.40^{e}	115.4 ± 4.17^{b}	1417.91 ± 11.16^{c}	1608.55 ± 6.25^{c}
8	2.91 ± 0.16^{c}	50.00 ± 4.05^{d}	195.80 ± 6.31^{d}	93.37 ± 4.21^{d}	133.6 ± 5.11^{a}	1088.21 ± 4.19^{d}	1315.18 ± 7.56^{d}
10	2.48 ± 0.34^{cd}	41.83 ± 2.92^{e}	186.46 ± 2.99^{d}	105.25 ± 3.22^{c}	114.71 ± 3.42^{b}	829.41 ± 4.81^{e}	1049.37 ± 5.28^{e}
12	1.95 ± 0.13^{d}	33.57 ± 1.51^{f}	163.23 ± 7.05^{e}	127.61 ± 5.27^{a}	89.74 ± 2.40^{d}	635.05 ± 8.62^{f}	852.4 ± 4.33^{f}
14	1.23 ± 0.28^{e}	27.92 ± 0.97^{fg}	145.35 ± 6.31^{f}	115.29 ± 4.12^{b}	92.35 ± 2.11^{e}	415.83 ± 4.36^{g}	623.48 ± 5.25^{g}
16	1.07 ± 0.18^{e}	22.73 ± 1.38^{gh}	126.09 ± 3.15^{g}	96.06 ± 5.44^{d}	50.98 ± 1.17^{f}	291.71 ± 6.90^{h}	438.74 ± 3.28^{h}
18	0.86 ± 0.12^{e}	18.58 ± 2.15^{h}	-	70.61 ± 5.37^{e}	32.73 ± 4.25^{g}	-	103.35 ± 3.22^{i}
20	0.69 ± 0.05^{e}	-	-	40.99 ± 3.30^{g}	-	-	40.99 ± 2.13^{j}

[1] Values are means ± standard deviation (n = 3). [2] Different letters in the same column indicate a significant difference ($p < 0.05$).

Table 4. Changes in relaxation time and peak area of *G. elata* dried at 80 °C after steaming.

Drying Time (min)	T_{21} (ms) [1,2]	T_{22} (ms) [1,2]	T_{23} (ms) [1,2]	A_{21}/g [1,2]	A_{22}/g [1,2]	A_{23}/g [1,2]	A_{Total}/g [1,2]
2	4.20 ± 0.14^{a}	73.84 ± 4.06^{a}	226.27 ± 5.32^{a}	57.68 ± 1.93^{d}	91.08 ± 4.04^{c}	2026.95 ± 6.34^{a}	2175.71 ± 9.82^{a}
4	3.70 ± 0.49^{a}	65.46 ± 3.67^{b}	209.65 ± 4.18^{b}	72.70 ± 4.75^{c}	114.61 ± 3.13^{b}	1546.24 ± 10.91^{b}	1733.55 ± 8.43^{b}
6	2.97 ± 0.22^{b}	55.10 ± 3.72^{c}	198.94 ± 5.81^{b}	90.58 ± 7.13^{b}	125.40 ± 3.99^{a}	1136.94 ± 11.04^{c}	1352.92 ± 7.26^{c}
8	2.47 ± 0.24^{bc}	46.34 ± 4.36^{d}	185.32 ± 4.90^{c}	113.37 ± 5.79^{a}	116.93 ± 4.75^{b}	774.60 ± 6.61^{d}	1004.9 ± 5.25^{d}
10	1.98 ± 0.18^{cd}	37.17 ± 1.93^{e}	166.81 ± 3.20^{d}	96.92 ± 4.59^{b}	88.04 ± 2.04^{c}	570.56 ± 5.58^{e}	755.52 ± 6.47^{e}
12	1.64 ± 0.24^{d}	28.57 ± 1.38^{f}	143.23 ± 7.05^{e}	79.28 ± 2.89^{c}	63.07 ± 2.58^{d}	269.21 ± 4.21^{f}	411.56 ± 5.23^{f}
14	1.03 ± 0.15^{e}	21.58 ± 3.70^{f}	-	55.96 ± 4.15^{d}	35.67 ± 3.69^{e}	-	91.62 ± 4.22^{g}
16	0.93 ± 0.22^{e}	-	-	35.39 ± 3.51^{e}	-	-	35.39 ± 3.21^{h}

[1] Values are means ± standard deviation (n = 3). [2] Different letters in the same column indicate a significant difference ($p < 0.05$).

The signal amplitude of the T_2 proton relaxation time was standardized against the sample mass, giving A_{21}/g, A_{22}/g, A_{23}/g, and A_{total}/g, which represent the signal amplitude per mass of bound water, immobilized water, free water, and total water, respectively [28].

As the area under the signal peak was proportional to the water content, it can be used to estimate the sample water content. The A_{total}/g values continued to decline with increasing drying time, which indicated that water always moved in the direction of poor mobility. Furthermore, higher temperatures resulted in faster movement. The A_{23}/g values decreased similarly to the A_{total}/g values, which indicated that free water had the highest mobility and was removed first in the drying process. Changes in the A_{22}/g values showed no obvious pattern, possibly owing to cell membrane damage caused by drying and the irregular movement of immobilized water. The A_{21}/g values initially increased and then decreased in the drying process, which might be due to free water and immobilized water moving in the direction of poor mobility with increasing drying time, thus increasing the bound water content. After drying for 16 h, the contents of all three water states decreased, and only bound water remained at the end of drying.

2.3. MRI Analysis of G. Elata during Drying

As a fast and nondestructive analytical technology, MRI can analyze the internal structure and water states of samples during the drying process. Figure 4 shows vertical-sectional and cross-sectional MRI images of *G. elata* during the drying process. The color strip shows that different colors represent different proton densities and indirectly reflect moisture content. As shown in Figure 4, the color of the image was consistent after steaming *G. elata*, indicating that the water distribution was uniform. As the drying time increased, the yellow area decreased and the green area increased, indicating that moisture was continuously lost during the drying process. The proton density decreased from the outside to the inside, as previously observed in dried eggplant [29]. After drying for 16 h, the MRI image became barely visible, demonstrating that most of the water had evaporated, leaving only bound water that was tightly linked to the macromolecules.

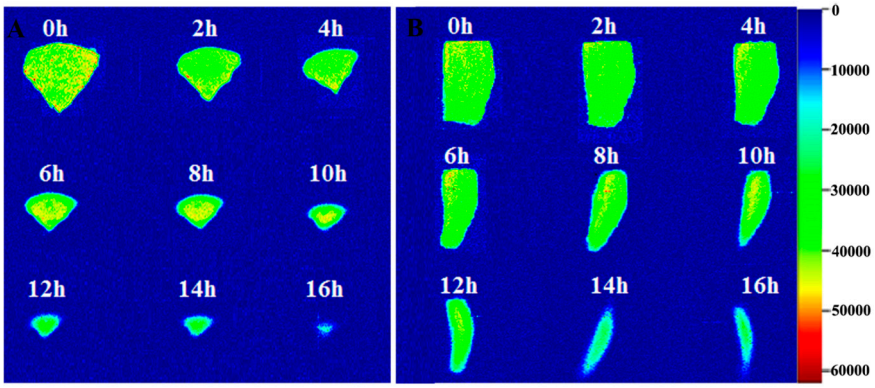

Figure 4. Vertical-sectional (**A**) and cross-sectional (**B**) MRI images of *G. elata* during the drying process at 60 °C.

2.4. Change in the Color of G. elata at Different Drying Temperatures

The color of dry *G. elata* is another important indicator for evaluating herb quality. The impact of temperature on the color parameters (L^*, a^*, b^*) is shown in Figure 5 L^* values (lightness) decreased as the drying temperature increased (40, 60, and 80 °C), while b^* values (yellowness) increased gradually, and a^* values (redness) were significantly higher at 80 °C. These results might be attributed to the occurrence of Maillard browning reactions [30]. Therefore, it is advisable to use lower temperatures during the drying processing to ensure the quality of dried *G. elata* appearance is maintained.

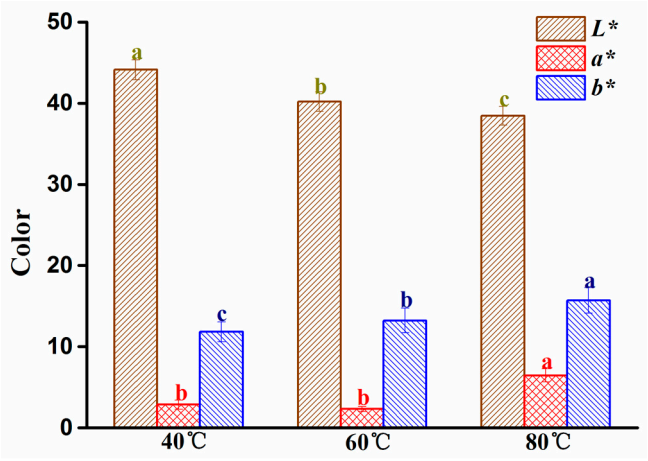

Figure 5. Effect of temperature on color parameters *L**, *a**, and *b**. Different letters in the same color column indicate significant difference at $p < 0.05$.

2.5. Correlation Analysis

As a fast and nondestructive analytical technique, NMR technology can replace some time-consuming methods if the relationships between NMR parameters and relative physicochemical parameters are determined. Relationships among moisture content (MC), LF-NMR parameters, and color parameters were investigated using linear analysis, with the corresponding correlation coefficients shown in Table 5. MC showed very significant correlations with T_{21}, T_{22}, A_{23}/g, and A_{Total}/g, with coefficients of 0.982, 0.980, 0.990, and 0.996, respectively. Similarly, *L** showed very significant correlations with A_{23}/g and A_{total}/g, while *b** showed significant correlations with T_{22} and T_{23}. No significant correlation was found between *a** and the NMR parameters in the *G. elata* samples. These results showed that LF-NMR was not only able to measure the moisture content, but also reflected the color of the medicinal material, which can reflect its overall quality.

Table 5. Correlation coefficients among moisture content (MC), LF-NMR parameters, and color parameters.

	T_{21}	T_{22}	T_{23}	A_{21}/g	A_{22}/g	A_{23}/g	A_{Total}/g
MC	0.982 *	0.980 **	0.972 *	0.233	0.131	0.991 **	0.996 **
*L**	−0.162	−0.628	−0.729	0.527	0.521	0.904 **	0.913 **
*a**	0.017	−0.219	0.228	0.509	0.432	0.613	0.722
*b**	0.728	0.823 *	0.845 *	0.749	0.071	0.769	0.776

* $p < 0.05$, significant at the 0.05 level, ** $p < 0.01$, significant at the 0.01 level.

2.6. Establishment of the PLSR Model

A strong correlation was found between A_{total}/g and MC. Therefore, the linear equations can predict the moisture content in *G. elata*. However, as reported by Li et al. [31], the NMR parameters of T_2 curves were extremely collinear. Therefore, it is necessary to establish a more reliable prediction method.

As a reliable and convenient multivariate regression method, PLSR is well-suited to solving multicollinearity problems [32]. Figure 6A shows the relationship between the RMSEV of calibration and rank values, which clearly showed that the best rank value was 6. From the best rank value, predicted values vs. measured values of MC were obtained using the PLSR model. R^2_c, R^2_{cv}, RMSEC, RMSEV, and RPD were used to evaluate the model. The PLSR model for MC gave R^2_c and R^2_{cv} values of 0.994 and 0.993, with RMSEC and RMSEV values of 2.07 and 2.16, while the RPD value was 12.7. These results indicated that PLSR analysis, which accounted for all NMR parameters, also showed

good correlations among these parameters. All results demonstrated that LF-NMR was a feasible and convenient method for monitoring moisture content.

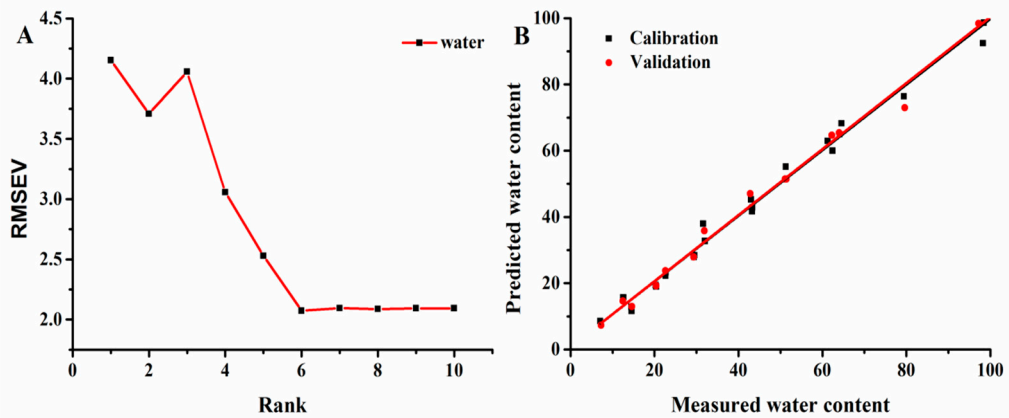

Figure 6. RMSEV of calibration vs. (**A**) rank values and (**B**) the measured and predicted plots of the PLSR models for water in *G. elata* samples.

3. Experimental

3.1. Sample Preparation

Fresh *G. elata* (second class *Gastrodia elata* f. glauca) used in this study was purchased from the Xiaocaoba Gastrodia Planting Base in Shaotong City (Shaotong, Yunnan Province, China) and stored in a refrigerator at 4 °C before use. Before each experiment, *G. elata* was washed and steamed for 10 min in a steamer (Qiaojieer Electric Co. Ltd., Zibo, Shandong, China). After steaming, the *G. elata* tuber was cut into pieces approximately 4 cm in height and 1 cm in radius with 90° curvature. The weight of each *G. elata* tuber sample was approximately 10 ± 0.5 g.

3.2. Moisture Content Measurement

The initial moisture content (MC) was calculated using Equation (1):

$$\mathrm{MC} = \frac{W_0 - W}{W} \quad (1)$$

where W_0 (g) is the initial mass and W (g) is the constant mass after drying at 105 °C.

3.3. Drying Process

G. elata tuber samples were laid flat on a metal grid tray and placed in an infrared-forced circulation drying oven (Wujiang Huafei Electric Heating Equipment Co. Ltd., Suzhou, China). The samples were dried at 40, 60, or 80 °C with a constant air velocity of 1 m/s over the tray. The samples were weighed every 30 min for the first hour, and then every 1 h until the change in weight between measurements was less than 0.01 g. All experiments were performed in triplicate.

3.4. LF-^{1}H NMR Measurements

LF-^{1}H NMR measurements were performed using an NMR Analyzer (MesoMR23-060H-I, Niumag Corp., Shanghai, China) equipped with a 0.5 T permanent magnet corresponding to a proton resonance frequency of 20 MHz at 32 °C. The *G. elata* tuber samples were placed in an NMR tube with an outer diameter of 25 mm. The proton decay signals were collected using the Carr–Purcell–Meiboom–Gill pulse sequence (CPMG) with a τ-value (time between 90° pulse and 180° pulse) of 200 μs, and 90° and 180° pulses of 7.5 and 15 μs, respectively. The NMR measurement

parameters were set as follows: Echo time (TE), 0.35 ms; waiting time (TW), 2000 ms; data from 18,000 echoes acquired using 8 repeated scans.

Relaxation time analysis and distributed exponential curve fitting were performed using MultiExp Inv Analysis software (Niumag Corp., Shanghai, China). Multiexponential fitting analysis was performed on the relaxation data using a modified inversion algorithm to obtain improved fitting. The relaxation time and its corresponding water population (area ratio) from this analysis were recorded.

3.5. MRI Detection

MRI was performed using an NMR Analyzer (MesoMR23-060H-I, Niumag Corp., Shanghai, China) equipped with a 25-mm radio frequency coil at 32 °C. The MRI measurement parameters were set as follows: Slice width, 3 mm; slice gap, 1 mm; TR (time repetition), 2000; TE (time echo), 25 ms; average, 4.

3.6. Color Analysis

The fracture surface color of *G. elata* was measured using an NH310 high-quality portable colorimeter (Shenzhen 3NH Technology Co. Ltd., Shenzhen, China). The color was described in terms of L^*, a^*, and b^*, where L^* is lightness (0 for black, 100 for white), a^* is green to red, and b^* is blue to yellow. All experiments were performed in triplicate.

3.7. Statistical Analysis

Data are reported as means ± standard deviation. The moisture content, transverse relaxation time, and signal amplitude were calculated using the Statistical Package for the Social Sciences version 17.0 (SPSS Inc., Chicago, IL, USA). One-way analysis of variance (ANOVA) was used to determine whether differences between the mean values were significant. Origin 9 (OriginLab Corp., Northampton, MA, USA) was used to produce the figures. PLSR analysis was performed using Unscrambler 9.7 (Camo Software AS, Oslo, Norway). The performance of the PLSR model can be evaluated using the determination coefficients of calibration (R^2_C) and cross-validation (R^2_{CV}), and the root mean square errors of calibration (RMSEC) and cross-validation (RMSECV). In general, a good model should have high R^2_C and R^2_{CV} values, and low RMSEC and RMSECV values.

4. Conclusions

This study indicates that the LF-NMR and MRI method is feasible for monitoring water variation in *G. elata* samples during the drying process. Three water states (bound, immobilized, and free) in *G. elata* samples were investigated using multiexponential fitting and inversion of the NMR data. LF-NMR reflected the variation in water states in *G. elata* samples during drying, while MRI reflected the spatial distribution of water and structural changes. Significant correlations were found among MC, L^*, b^*, and NMR parameters. PLSR analysis, taking into account all NMR parameters, also showed good correlations among these parameters. These results suggested that LF-NMR was a feasible and convenient method for monitoring moisture content. This demonstrates that LF-NMR and MRI can monitor the drying process of *G. elata*, and has great potential for application to other Chinese herbal medicines.

Author Contributions: Y.C. conducted the experiment and wrote the paper; H.D. and J.L. conducted the experiment; L.G. and X.W. designed and guided the experiment.

Funding: This work was financially supported by Key project at central government level: The ability establishment of sustainable use for valuable Chinese medicine resources (2060302), the National Key Research and Development Program of China (NO. 2017YFC1700703), and the Key Research and Development Program of Shandong Province (NO. 2016GSF202014).

Acknowledgments: We thank Simon Partridge, from Liwen Bianji, for editing the English text of a draft of this manuscript.

Conflicts of Interest: The authors declare no conflict and interest.

References

1. Xu, W.; Li, J.; Song, F.; Li, Z.; Zhang, Z. Research Process of the Drying Technology of Chinese Herbal Medicine. *Med. Plant* **2014**, *5*, 8–11.
2. Yan, D.; Yuan, X.; Xie, D.; Hu, M.; Li, M.; Liu, Y.; Wu, C. Research status and thoughts on sterilization of Chinese herbal medicine pieces. *Tradit. Herb. Drugs* **2016**, *47*, 1425–1428.
3. Segtnan, V.H.; Sasic, S.; Isaksson, T.; Ozaki, Y. Studies on the Structure of Water Using Two-Dimensional Near-Infrared Correlation Spectroscopy and Principal Component Analysis. *Anal. Chem.* **2001**, *73*, 3153–3161. [CrossRef]
4. Lee, D.J. Measurement of Bound Water Content in Sludge: The Use of Differential Scanning Calorimetry (DSC). *J. Chem. Technol. Biotechnol* **1995**, *62*, 359–365. [CrossRef]
5. Zhang, Q.Q.; Li, W.; Li, H.K.; Chen, X.H.; Jiang, M.; Dong, M.S. Low-field nuclear magnetic resonance for online determination of water content during sausage fermentation. *J. Food Eng.* **2017**, *212*, 291–297. [CrossRef]
6. Li, T.; Tu, C.; Ru, X.; Gao, Y.; Li, W.; Wang, K.; Xiao, Y.; Dong, M. Study of Water Dynamics in the Soaking, Steaming, and Solid-State Fermentation of Glutinous Rice by LF-NMR: A Novel Monitoring Approach. *J. Agric. Food Chem.* **2015**, *63*, 3261–3270. [CrossRef] [PubMed]
7. Shao, X.; Li, Y. Application of Low-Field NMR to Analyze Water Characteristics and Predict Unfrozen Water in Blanched Sweet Corn. *Food Bioprocess Technol.* **2013**, *6*, 1593–1599. [CrossRef]
8. Yang, S.; Liu, X.; Jin, Y.; Li, X.; Chen, F.; Zhang, M.; Lin, S. Water Dynamics in Egg White Peptide, Asp-His-Thr-Lys-Glu, Powder Monitored by Dynamic Vapor Sorption and LF-NMR. *J. Agric. Food Chem.* **2016**, *64*, 2153–2161. [CrossRef] [PubMed]
9. Rao, W.; Wang, Z.; Shen, Q.; Li, G.; Song, X.; Zhang, D. LF NMR to explore water migration and water protein interaction of lamb meat being air dried at 35 °C. *Drying Technol.* **2018**, *36*, 366–373. [CrossRef]
10. Sánchez-Alonso, I.; Moreno, P.; Careche, M. Low field nuclear magnetic resonance (LF-NMR) relaxometry in hake (*Merluccius merluccius*, L.) muscle after different freezing and storage conditions. *Food Chem.* **2014**, *153*, 250–257. [CrossRef]
11. Ghosha, P.K.; Jayasa, D.S.; Gruwel, M.L.H.; White, N.D.G. A magnetic resonance imaging study of wheat drying kinetics. *Biosyst. Eng.* **2007**, *97*, 189–199. [CrossRef]
12. Geng, S.; Wang, H.; Wang, X.; Ma, X.; Xiao, S.; Wanga, J.; Tan, M. A non-invasive NMR and MRI method to analyze the rehydration of dried sea cucumber. *Anal. Methods* **2015**, *7*, 2413–2419. [CrossRef]
13. Wu, J.; Li, Y.; Gao, X. Monitoring a typical fermentation process of natto by low-field nuclear magnetic resonance (LF-NMR) and magnetic resonance imaging (MRI) techniques. *Anal. Methods* **2016**, *8*, 7134–7140. [CrossRef]
14. Cheng, S.; Tang, Y.; Zhang, T.; Song, Y.; Wang, X.; Wang, H.; Wang, H.; Tan, M. Approach for monitoring the dynamic states of water in shrimp during drying process with LF-NMR and MRI. *Drying Technol.* **2018**, *36*, 841–848. [CrossRef]
15. Xu, F.; Jin, X.; Zhang, L.; Chen, X.D. Investigation on water status and distribution in broccoli and the effects of drying on water status using NMR and MRI methods. *Food Res. Int.* **2017**, *96*, 191–197. [CrossRef]
16. Matias, M.; Silvestre, S.; Falcão, A.; Alves, G. *Gastrodia elata* and epilepsy: Rationale and therapeutic-potential. *Phytomedicine* **2016**, *26*, 1511–1526. [CrossRef] [PubMed]
17. Teo, C.C.; Tan, S.N.; Yong, J.W.H.; Hew, C.S.; Ong, E.S. Evaluation of the extraction efficiency of thermally labile bioactive compounds in Gastrodia elata Blume by pressurized hot water extraction and microwave-assisted extraction. *J. Chromatogr. A* **2008**, *1182*, 34–40. [CrossRef]
18. Chen, W.C.; Lai, Y.S.; Lin, S.H.; Lu, K.H.; Lin, Y.E.; Panyod, S.; Ho, C.T.; Sheen, L.Y. Anti-depressant effects of *Gastrodia elata* Blume and its compounds gastrodin and 4-hydroxybenzyl alcohol, via the monoaminergic system and neuronal cytoskeletal remodeling. *J. Ethnopharmacol.* **2016**, *182*, 190–199. [CrossRef]
19. Wong, H.Y.; Hu, B.; So, P.K.; Chan, C.O.; Mok, D.K.W.; Xin, G.Z.; Li, P.; Yao, Z.P. Rapid authentication of Gastrodiae rhizoma by direct ionization mass spectrometry. *Anal. Chim. Acta* **2016**, *938*, 90–97. [CrossRef]
20. Shan, M.; Qian, Y.; Yu, S.; Zhang, L.; Ding, A. Study on integrative technology of primary processing for Gastrodiae Rhizoma based on response surface methodology. *Chin. Tradit. Herb. Drugs* **2016**, *47*, 420–424.

21. Tian, Z.; Wang, J.; Liu, J.; Dai, K.; Liu, X.; Yu, X.; Ma, C.; Liu, D. Effects of Different Processsing Methods and Steamed Time on Quality of Zhaotong Gastrodiae rhizoma. *Southwest Chin. J. Agric. Sci.* **2016**, *29*, 1701–1706.
22. Raffo, A.; Gianferri, R.; Barbieri, R.; Brosio, E. Ripening of banana fruit monitored by water relaxation and diffusion ^{1}H-NMR measurements. *Food Chem.* **2005**, *89*, 149–158. [CrossRef]
23. Chen, L.; Tian, Y.; Sun, B.; Wang, J.; Tong, Q.; Jin, Z. Rapid, accurate, and simultaneous measurement of water and oil contents in the fried starchy system using low-field NMR. *Food Chem.* **2017**, *233*, 525–529. [CrossRef] [PubMed]
24. Wang, H.H.; Wang, R.Y.; Song, Y.K.; Kamal, T.; Lv, Y.; Zhu, B.W.; Tao, X.H.; Tan, M.Q. A fast and non-destructive LF-NMR and MRI method to discriminate adulterated shrimp. *J. Food Meas. Charact.* **2018**, *12*, 1340–1349. [CrossRef]
25. Tan, M.; Lin, Z.; Zu, Y.; Zhu, B.; Cheng, S. Effect of multiple freeze-thaw cycles on the quality of instant sea cucumber: Emphatically on water status of by LF-NMR and MRI. *Food Res. Int.* **2018**, *109*, 65–71. [CrossRef] [PubMed]
26. Wei, S.; Tian, B.Q.; Jia, H.F.; Zhang, H.Y.; He, F.; Song, Z. Investigation on water distribution and state in tobacco leaves with stalks during curing by LFNMR and MRI. *Drying Technol.* **2018**, *4*, 1–8. [CrossRef]
27. Mothibe, K.J.; Zhang, M.; Mujumdar, A.S.; Wang, Y.C.; Cheng, X.F. Effects of Ultrasound and Microwave Pretreatments of Apple Before Spouted Bed Drying on Rate of Dehydration and Physical Properties. *Drying Technol.* **2014**, *32*, 1848–1856. [CrossRef]
28. Li, M.; Wang, H.; Zhao, G.; Qiao, M.; Li, M.; Sun, L.; Gao, X.; Zhang, J. Determining the drying degree and quality of chicken jerky by LF-NMR. *J. Food Eng.* **2014**, *139*, 43–49. [CrossRef]
29. Adiletta, G.; Iannone, G.; Russo, P.; Patimo, G.; Pasquale, S.D.; Matteo, M.D. Moisture migration by magnetic resonance imaging during eggplant drying: A preliminary study. *Int. J. Food Sci. Technol.* **2014**, *49*, 2602–2609. [CrossRef]
30. Michalska, A.; Honke, J.; Łysiak, G.; Andlauer, W. Effect of drying parameters on the formation of early and intermediate stage products of the Maillard reaction in different plum (*Prunus domestica* L.) cultivars. *LWT Food Sci. Technol.* **2016**, *65*, 932–938. [CrossRef]
31. Li, L.; Zhang, M.; Bhandari, B.; Zhou, L. LF-NMR online detection of water dynamics in apple cubes during microwave vacuum drying. *Drying Technol.* **2018**, 1–10. [CrossRef]
32. Zheng, H.; Lu, H. Use of kinetic, Weibull and PLSR models to predict the retention of ascorbic acid, total phenols and antioxidant activity during storage of pasteurized pineapple juice. *LWT Food Sci. Technol.* **2011**, *44*, 1273–1281. [CrossRef]

Sample Availability: Samples are available from the authors.